Construction and Building Materials 411 (2024) 134634

Contents lists available at ScienceDirect

Construction and Building Materials

journal homepage: www.elsevier.com/locate/conbuildmat

Review

Inelastic buckling of reinforcing bars: A state-of-the-art review of existing models and opportunities for future research

Mohammad M. Kashani

Faculty of Engineering and Physical Sciences, University of Southampton, Southampton, UK

ARTICLE INFO

Keywords:
Reinforcing bars
Reinforced concrete
Buckling
Corrosion
Low-cycle fatigue

ABSTRACT

Despite the substantial steps made in understanding the mechanics of reinforced concrete structures, effectively addressing, and mitigating inelastic buckling remains a complex and enduring challenge. Consequently, this paper provides a comprehensive review of all the previous studies on modelling the inelastic buckling of reinforcing bars, and the capability of current state-of-the-art numerical models to simulate the nonlinear stress-strain response of reinforcing bars with the effect of buckling under monotonic and cyclic loading. This review paper consists of four different clusters including: (i) inelastic buckling of reinforcing bars under monotonic loading with and without corrosion, (ii) inelastic buckling of reinforcing bars under cyclic loading with and without corrosion, (iii) influence of inelastic buckling on low-cycle fatigue life of reinforcing bars with and without corrosion, and (iv) influence of tie reinforcement on global stability of longitudinal bars and buckling length calculation. For each group, a summary and critical review of all the previous research is provided. A quantitative comparison between the most widely used uniaxial material models have been made and their performance have been assessed against experimental data. Finally, the current limitations in existing literature are examined, unresolved issues for future research are identified, and some recommendations for future research are suggested.

1. Introduction

In the context of analysing nonlinear performance of reinforced concrete (RC) structures under seismic loads, the common practice involves employing fibre-type section models [1,2]. These models are utilised to replicate the flexural behaviour of beams, columns, and walls, which experience nonlinear responses [3]. Typically integrated into plastic hinge or distributed-plasticity beam-column elements [1,2], these fibre-type section models have been implemented in software tools like OpenSees [4], SeismoStruct [5], and SAP2000 [6]. With the use of a fibre-type section model, the cross section of a structural element is divided into multiple steel and concrete fibres. These fibres collectively represent the behaviour of the material. The nonlinear characteristics of the materials are captured through uniaxial constitutive models for steel, as well as for confined and unconfined concrete. Consequently, the accuracy of this modelling approach heavily relies on the precision of these uniaxial constitutive models.

Previous studies have indicated that fibre-type section models, which include both lumped and distributed plasticity elements, is capable of simulating the stiffness, strength, and cyclic behaviour of RC components when subjected to moderate levels of deformation [7–9]. However, limited attention has been devoted to comprehensively simulating the response to the reduction in lateral load-bearing capacity, and more critically, axial load-bearing capacity [3,9,10]. Additionally, there is a limited body of work that showcases the precise emulation of drift capacity, which signifies the point where substantial loss in lateral strength becomes evident [3]. When RC members experience flexural loading, the decline in strength typically stems from factors such as the buckling of longitudinal reinforcement, fracture of longitudinal reinforcement due to either large tensile strain or the effect of low-cycle, high-amplitude fatigue, and/or the crushing of the confined concrete core [10].

Over the past few decades, several researchers have examined the cyclic performance of reinforcing steel with and without the effect of inelastic buckling [11–20]. Their focus has centred on simulating the behaviour of reinforcing steel that remains free from corrosion. However, it is important to note that numerous critical structures are situated in regions prone to high seismic activity and are also exposed to corrosive surroundings. Recent experimental investigations, which examine the nonlinear cyclic performance of RC elements featuring

E-mail address: mehdi.kashani@soton.ac.uk.

https://doi.org/10.1016/j.conbuildmat.2023.134634
Received 24 September 2023; Received in revised form 27 November 2023; Accepted 14 December 2023
Available online 22 December 2023

corroded reinforcement, reveal a substantial influence of corrosion on the response of such structures [21–29]. The empirical findings highlight that corrosion results in a change in the failure mechanism of RC components subjected to flexural loading. In certain instances, pronounced buckling phenomena were detected, arising from the combined impact of uneven pitting corrosion along the longitudinal reinforcement and corrosion affecting the horizontal/transverse ties. Corrosion exerts a diminishing influence on the rigidity of transverse ties, which restrain the longitudinal bars against buckling. Once the corroded bars undergo buckling during cyclic loading, they fracture prematurely, especially under relatively lower levels of deformation. This premature fracture can be attributed to the combined influence of buckling and the non-uniform pitting corrosion, resulting in a substantial reduction of the low-cycle fatigue life of corroded RC elements subjected to cyclic loading [27].

1.1. Research contribution

As mentioned in the introduction, there are serval uniaxial material models available in the literature to simulate the inelastic buckling of bars with and without corrosion. Some of these models have been verified against experimental data and have been extensively used by other researchers. However, there is significant paucity in the literature to make a quantitative comparison between such models. Moreover, there are still some very important open issues in simulating inelastic buckling of uncorroded and corroded bars that needs further research. Therefore, there is a need for a comprehensive review paper that provides all this information in a single document that can be used in the future research by other researchers.

Accordingly, the review paper presented here focusses on experimental testing, numerical modelling, and uniaxial material models of reinforcing bars subject to monotonic and cyclic loading (with and without corrosion). The primary objective of this paper is to compile all the relevant and significant information dispersed in the literature into a single comprehensive document, offering a critical review of these models. Finally, the paper concludes by pinpointing unresolved matters and research gaps, and identifies the areas for future research within this domain.

2. Inelastic buckling of reinforcing bars under monotonic loading

2.1. Modelling inelastic buckling behaviour of reinforcing bar without the effect of corrosion

Table 1, shows a summary of previous studies on inelastic buckling of reinforcing bars under monotonic loading. The dataset is extracted from a variety of literature sources comprises a large number of distinct reinforcing bar specimens. These specimens were chosen to cover a range of scenarios. First, the unsupported length ratios, which compares the length of the bar (L) to its diameter (D) known as L/D ratio, vary from 5 to 20. Second, the yield strengths of the bars, from 295 MPa to 540 MPa. Lastly, the ultimate strength-to-yield strength ratios, range from 1.2 to 1.6. For additional information about the experimental dataset and all the associated parameters, you can refer to Table A1 in the appendix.

Several researchers, as outlined in Table 1, have developed uniaxial material models that can be used in nonlinear finite element analysis of RC structures.

The early models in Table 1 [30–36] were mainly focused analytical modelling and experimental testing of reinforcing bars to investigate the inelastic buckling phenomenon. The first ever uniaxial material model that is available in the literature to simulate the inelastic buckling of reinforcing bars is Mont-Nuti [13], which was published in 1992. The historical development of uniaxial models to simulate the inelastic buckling of bars are discussed in the following sections of this paper.

Table 1
Previous studies on modelling inelastic buckling of reinforcing bars under monotonic loading.

Reference	Year of Study	Type of Study
Shanley 1947[30,31]	1947, 1950	Analytical modelling
Bresler and Gilbert[32]	1961	Analytical modelling
Johnston[33]	1961	Analytical modelling
Mander et al.[34]	1984	Experimental testing and analytical modelling
Mau and El-Mabsout [35]	1989	Analytical modelling
Papia et al.[36]	1989	Analytical modelling
Monti and Nuti[13]	1992	Experimental testing and uniaxial material model
Gomes and Appelton [15]	1997	Material model
Bayrak and Sheikh[37]	2001	Experimental testing and analytical modelling
Dhakal and Maekawa [38,39]	2002	Numerical modelling and uniaxial material model
Bae et al.[40]	2005	Experimental testing and uniaxial material model
Cosenza and Prota[41]	2006	Experimental testing and uniaxial material model
Gil-Martín et al.[42]	2008	Analytical modelling
Massone and Moroder [43]	2009	Analytical modelling
Prota e t al.[16]	2009	Experimental testing
Urmson and Mander [44]	2012	Analytical modelling
Kashani et al.[45,46]	2013, 2015	Experimental testing and analytical modelling
Zong et al.[20,47]	2010 and 2014	Material model
Massone and Lopez[48]	2014	Material model
Imperatore and Rinaldi [49]	2019	Experimental testing and analytical modelling

Here, the relevant equations of most widely used models and their parameters are presented, and a comparison between these models with experimental data are provided.

2.1.1. Monti–Nuti model

Monti-Nuti model [13] is one of the very first uniaxial material models developed for inelastic buckling of reinforcing bars. In this model for the unsupported length ratio (L/D) of 5, the compressive monotonic curve practically aligns with the tensile curve, indicating that the bar maintains a straight form. When $L/D = 8$, a brief overlap region arises, including a superposition length of $\gamma_s = \varepsilon_{5\%} - \varepsilon_y$. Here, ε_y is the yield strain, and $\varepsilon_{5\%}$ signifies the strain where the compressive curve diverges by more than 5% from the tensile curve, trending toward lower values. In the case of $L/D = 11$, once the yield point is reached, the onset of buckling becomes evident, leading to a retreat of the compressive monotonic curve from the tensile counterpart ($\gamma_s = 0$).

This behaviour is describes with an empirical relationship found for γ_s:

$$\gamma_s = \frac{11 - \frac{L}{D}}{e^{c(L/D)} - 1} \geq 0 \text{ , for} 5 < \frac{L}{D} \leq 11 \quad (1)$$

where $c = 0.5$ calibrated from experimental data.The hardening ratio, denoted as b, is $b = E_p/E_0$ (b^+ for the tensile branch, b^- for the compressive branch). Here, E_p represents the post-yielding modulus, while E_0 is the initial elastic modulus. In experimental observations, inelastic buckling starts to manifest when the unsupported length ratio (L/D) surpasses a critical threshold of $(L/D)_{cr} = 5$. Following the occurrence of yielding, a softening branch ($b^- < 0$) becomes evident. This softening branch (b^-) decreases as the unsupported length ratio (L/D) increases and is not influenced by the hardening ratio (b^+) of the material. As a result, the definition of b^- is as follows:

$$b^{-} = a\left[\left(\frac{L}{D}\right)_{cr} - \frac{L}{D}\right], \text{for} \frac{L}{D} > \left(\frac{L}{D}\right)_{cr} \quad (2)$$

where, the parameter a is calibrated using the experimental. $a = 0.006$ results in the secant slope ratio (from ε_y to $\varepsilon = 10\varepsilon_y$), while $a = 0.008$ gives the initial tangent slope ratiob_0^+. The softening branch converge to an asymptotic value of$\sigma_\infty = \frac{6\sigma_y}{\frac{L}{D}}$. Where σ_y = yield strength. It is noted that with increasing L/D ratio softening branches resulted in lower values ofσ_∞.

In summary, this model is calibrated using experimental data of bars with $D = 16$, 20, 24 mm and $L/D = 5$, 8, 11, and hence, does not cover bars with large L/D ratios. Furthermore, since the model is purely based on limited experimental data, the softening branch does not account for influence of yield strength and hardening ratio of the material. Further discussion on the performance of this model and comparison with experimental data is available in Section 2.1.8.

2.1.2. Gomes–Appleton model

The Gomes–Appleton model [15] characterises the mean stress–-strain correlation, formulated on the basis of the equilibrium attained by a buckled reinforcing bar constrained by two consecutive hoops. As per the findings of Gomes and Appleton's investigation, when strain remains small, it is crucial to consider the interaction between the axial load N and the plastic bending moment M_p to accurately compute the stress of the buckled reinforcing bar. However, as strain magnitudes increase (e.g. from 0.5% to 1.0%), it becomes permissible to neglect the N–M_p interaction without significantly compromising precision. Given that the compressive strain at the initiation of buckling, following a significant strain reversal, Gomes and Appleton proposed that for simplicity, one could omit consideration of the N–M_p interaction. In this context, assuming an average strain ε_s and an average stress σ_s for a reinforcing bar positioned between two successive hoops, ε_s can be defined as δ/L, while σ_s can be established as N/A_s. Here, δ and N denote axial deformation and axial load, respectively, L is the spacing between two consecutive hoops, and A_s represents the cross-sectional area of the reinforcing bar. Then the stress–strain relationship including buckling without consideration of N–M_p interaction is given by Eq. (3) below:

$$\sigma_s = \frac{2\sqrt{2} \times 0.424\sigma_y}{\frac{L}{D}} \frac{1}{\sqrt{\varepsilon_s}} \quad (3)$$

Further discussion on the performance of this model and comparison with experimental data is available in Section 2.1.8.

2.1.3. Cosenza–Prota model

Cosenza–Prota [41] conducted comprehensive research focused on experimental investigation of smooth bars under monotonic compression with different L/D ratios. The resulting stress-strain relationship is then made to cover a range of behaviours, starting from an elastic-plastic response similar to what's seen in tension when L/D is 5, and progressing to elastic buckling behaviour as L/D goes beyond 20.

In the proposed model the compressive stress-strain behaviour for $L/D \leq 5$ is identical to tension envelope and for $5 < L/D \leq 7$ is elastic-plastic. The post-buckling behaviour of bars with $8 \leq L/D \leq 20$ can be identified by three ranges of the stress-strain relationships. Firstly, an elastic behaviour up to yielding; secondly, a plateau; and finally, a nonlinear softening phase. The shift from the plateau to the onset of softening transpires at a specific strain value, denoted here as ε_s (with "s" indicating softening). This strain value is situated between ε_y (with "y" indicating yielding) and ε_h (with "h" indicating hardening). Based on experimental observations, ε_s can be determined using the following expression:

$$\frac{\varepsilon_s}{\varepsilon_y} = 1 + c_1 \frac{\varepsilon_h - \varepsilon_y}{\varepsilon_y} e^{\left(-c_2 \frac{L}{D}\right)} \quad (4)$$

where that $c_1 = 43.3$ and $c_2 = 0.47$. In Eq. (4) $\varepsilon_s \approx \varepsilon_y$ for $L/D = 20$ and $\varepsilon_s \approx \varepsilon_h$ for $L/D = 8$. The softening branch can be described by the following expression:

$$\sigma = \sigma_\infty + \left[(\sigma_y - \sigma_\infty) e^{-c_3\left(\frac{\varepsilon}{\varepsilon_s} - 1\right)}\right], \sigma_\infty = \sigma_y \frac{c_4}{\frac{L}{D}} \quad (5)$$

Where that $c_3 = 0.2$ and $c_4 = 2.8$. The value of σ_∞here is quite different from the suggested value by Monti and Nuti [13] for ribbed bars.

In summary, this model covers a wider range of L/D ratios and accounts for the influence of yield strength on post-buckling softening response. However, this model is only valid for smooth bars, and may not be directly applicable to ribbed bars.

2.1.4. Dhakal–Maekawa model

Dhakal and Maekawa [38] conducted nonlinear finite element analyses on individual reinforcement bars with varying L/D ratios, employing a fibre-based technique. Their empirical approach was based on the outcomes of these nonlinear analyses. They successfully developed a novel analytical model that can accurately simulate the post-yield buckling behaviour of reinforcing steel bars. Notably, the core principle of the model is the linkage between reinforcement buckling behaviour and the interaction of two key factors: the L/D ratio and the yield stress (σ_y) of the reinforcement material. Within this model, the compression response of the reinforcement is characterised by a single composite parameter termed the non-dimensional bar buckling parameter, denoted as λ_p. The definition of λ_p is provided in Eq. (6) as follows:

$$\lambda_p = \sqrt{\frac{\sigma_y}{100}} \frac{L}{D} \quad (6)$$

The σ_y in Eq. (5) is in MPa.Given non-dimensional stress $\eta = \sigma/\sigma_y$ and strain $\xi = \varepsilon/\varepsilon_y$ (where σ_y is the yield stress and ε_y is the yield strain) the following Eq.s define the stress-strain envelope.

$$\eta = \begin{cases} \xi; & \xi \leq 1 \\ \frac{(\eta_2 - 1)}{(\xi_2 - 1)}(\xi - 1) + 1; & 1 < \xi \leq \xi_2 \\ \eta_2 - 0.02\,(\xi - \xi_2)\,; & \xi_2 \leq \xi \& \eta \geq 0.2 \\ 0.2; & otherwise \end{cases} \quad (7)$$

where, the empirical relationships for (η_2,ξ_2) are given below:

$$\xi_2 = 55 - 2.3\,\lambda_p; \qquad \xi_2 \geq 7 \quad (8)$$

$$\eta_2 = \alpha\,(1.1 - 0.016\,\lambda_p)\,\eta_2^*; \qquad \eta_2 \geq 0.2 \quad (9)$$

Here, η^*_2 represents the non-dimensional piecewise stress linked to ξ_2. The parameter α carries significance as a softening coefficient and is contingent on the strain hardening characteristics of the reinforcement. In their study, Dhakal and Maekawa established that $\alpha = 0.75$ for elastic-perfectly plastic reinforcement, while for reinforcement exhibiting linear hardening, $\alpha = 1.0$. Further elaboration regarding the derivation of Eqs. (8) and (9) can be found in Dhakal and Maekawa's work [38]. Further discussion on the performance of this model and comparison with experimental data is available in Section 2.1.8.

2.1.5. Bae et al. model

Bae et al. [40] reported the findings from an experimental investigation focused on inelastic bar buckling behaviour. The programme entailed testing a total of 162 specimens of reinforcing bars subjected to monotonic compression loading. Moreover, a simple analytical model has been developed, designed to be integrated into the conventional cross section analysis methodology.

In this model the average axial strain is assumed as the summation of axial strain due to axial stress and axial strain from transverse

displacement of a bar after inelastic buckling; i.e. $\varepsilon_{ave} = \varepsilon_s + \varepsilon_{tra}$, where ε_{ave} is total average strain in a buckled bar, ε_s is the strain due to axial displacement, and ε_{tra} is the axial strain due to lateral displacement. The axial strain resulting from an axial stress can be calculated by referencing the tensile stress-strain curve. In this context, the stress-strain model for tension as suggested by Mander et al. [34] was employed as the basis for their post-buckling model. They proposed a set of equations to calculate the transverse displacement due to axial stress and subsequently axial strain due to transverse displacement. Further details are available in Bae et al.[40].

In summary, this model can simulate the post-buckling response of reinforcing bars. However, it requires several assumptions on initial imperfection and transverse displacement of reinforcing bars, which are difficult to be evaluated in all cases. Therefore, this model has not been widely used by other researchers.

2.1.6. Urmson and Mander model

Urmson and Mander [44] formulated a direct computational framework for simulating the axial compressive force-deformation steel reinforcement. This framework incorporated considerations of local buckling that occurs between successive tie reinforcement. The analysis of various L/D ratios resulted in some empirical interpretations, namely:

- At the onset of critical buckling load, the deformed bar exhibits notable tensile stress. At this pivotal section, a neutral axis (characterised by zero strain) is positioned $0.15D$ distant from the side experiencing tension.
- For extremely diminutive L/D ratios ($L/D < 4$), the inelastic local buckling capacity is governed by the ultimate compressive strength (plastic) of the section.
- At moderate L/D ratios (typically $4 < L/D < 11$), the inelastic local buckling capacity is influenced by lateral stability. Within this realm, and for a given yield strength of the steel, a consistent eccentricity (e/D ratio) is present. As an illustration, when $\sigma_y = 330$ MPa, e equals $0.125D$.

Following the above empirical observations, Urmson and Mander developed a formulation to predict both inelastic local buckling stress and strain depending on L/D ratio. Subsequently, a unified formula was suggested to capture the complete stress-strain behaviour in compression, accounting for strain-hardening and localised inelastic buckling. A compelling agreement was demonstrated between their computational model, and experimental data.

Although this model is quite accurate for small to medium L/D ratios, it has not been verified for $L/D > 11$. Therefore, the applicability of this model is limited to bar with $L/D < 11$.

2.1.7. Kashani et al. model

Kashani et al. [46] introduced a novel phenomenological uniaxial material model. This model was designed to simulate the behaviour of both corroded and uncorroded reinforcing bars including inelastic buckling and post-yield buckling phenomena. The model is calibrated using an extensive selection of experimental data involving both types of reinforcing bars. The model demonstrated its capability to capture the nonlinear post-buckling behaviour exhibited by both corroded and uncorroded bars. Notably, this model was built upon Dhakal and Maekawa's prior model. Consequently, the post-yield buckling response of reinforcing bars in this model can be expressed as a function of λ_p, as defined in Eq. (5).

In Kashani's model, the post-yield buckling response of reinforcing bars is characterised by an exponential function. The post-buckling curve is defined in Eq.s (10) to (13):

$$\sigma = \begin{cases} E_s\varepsilon & :\varepsilon \le \varepsilon_y \\ \sigma^* + (\sigma_y - \sigma^*)\exp\left(-\left(\rho_1 + \rho_2\sqrt{\varepsilon_p}\right)(\varepsilon_p)\right) & :\varepsilon > \varepsilon_y \end{cases} \quad \text{for } 8 \le L/D \le 30 \qquad (10)$$

$$\rho_1(\lambda_p) = 4.572\,\lambda_p - 74.43 \qquad (11)$$

$$\rho_2(\lambda_p) = 318.40\ \exp\ (-0.071\,\lambda_p) \qquad (12)$$

$$\sigma^* = 3.75\ \frac{\sigma_y}{\frac{L}{D}} \qquad (13)$$

where Es is the elastic modulus, ρ_1 is the initial tangent of the post-buckling response curve, ρ_2 is the rate of change of the tangent, ε is the current strain, $\varepsilon_p = \varepsilon - \varepsilon_y$ is the plastic strain, σ^* is the asymptotic lower stress limit of the post-buckling curve, and all other variables are as previously defined. This model improves the Dhakal and Maekawa's model by replacing the post-buckling trilinear curve with a smooth curve, which improves the numerical stability in nonlinear finite element simulations. Further discussion on the performance of this model and comparison with experimental data is available in Section 2.1.8.

2.1.8. Comparison of the most widely used post-buckling models for reinforcing bars

Fig. 1 shows a comparison between some of the most widely used material models against experimental data and nonlinear fibre element models of single reinforcing bars. The experimental data are taken from Kashani et al. [45,50] and nonlinear fibre element modelling data are taken from Kashani et al. [51].

The comparison of the model shows that there is a good agreement between the Dhakal-Maekawa and Kashani models and experimental and numerical data. However, Gomes-Appleton model is not very accurate bars with $L/D < 10$. This is because the formulation of Gomes-Appleton model is using plastic moment due to second order effects, and for simplicity the axial-flexure interaction is ignored. For bars with large L/D ratios this assumptions works well, however, in bars with smaller L/D ratios this assumption results in underestimating the stress in simulating the post-buckling softening response. The Monti-Nuti model does not show a good agreement with experimental and numerical results. This is because the original model is calibrated using a very limited experimental data.

2.2. Modelling inelastic behaviour of reinforcing bar with the effect of corrosion

2.2.1. Kashani et al. model

The impact of corrosion on the inelastic buckling of corroded bars was investigated by Kashani et al. [45] [50] experimentally and computationally [51]. Experimental testing and numerical simulations indicates that there are three main parameters that affect the buckling of corroded bars including (a) non-uniform loss of cross section area and second moment of area along the length of the bar, (b) changing the centroid of the bar cross section along of the bar, which results in eccentricity and (c) cross sectional shape of the bar, which is very important inelastic buckling. These parameters results in stress concentrations and impair imperfections, and subsequently, reduce the buckling capacity. Creating a precise equation that explains how corrosion affects the factors influencing buckling behaviour is challenging due to the complex nature of the problem and the unpredictable way corrosion happens. Therefore, Kashani et al. [45,46] proposed a set of empirical equations to modify the buckling and post-buckling behaviour of corroded bars.

The residual cross section of corroded bars can be estimated by assuming reduced cross section using Eq. (14) below:

$$D' = \frac{D_0}{10}\sqrt{100 - \psi} \qquad (14)$$

where, D' is the reduced bar diameter due corrosion, D_0 is the original bar diameter prior to corrosion, and ψ is the percentage of corrosion-

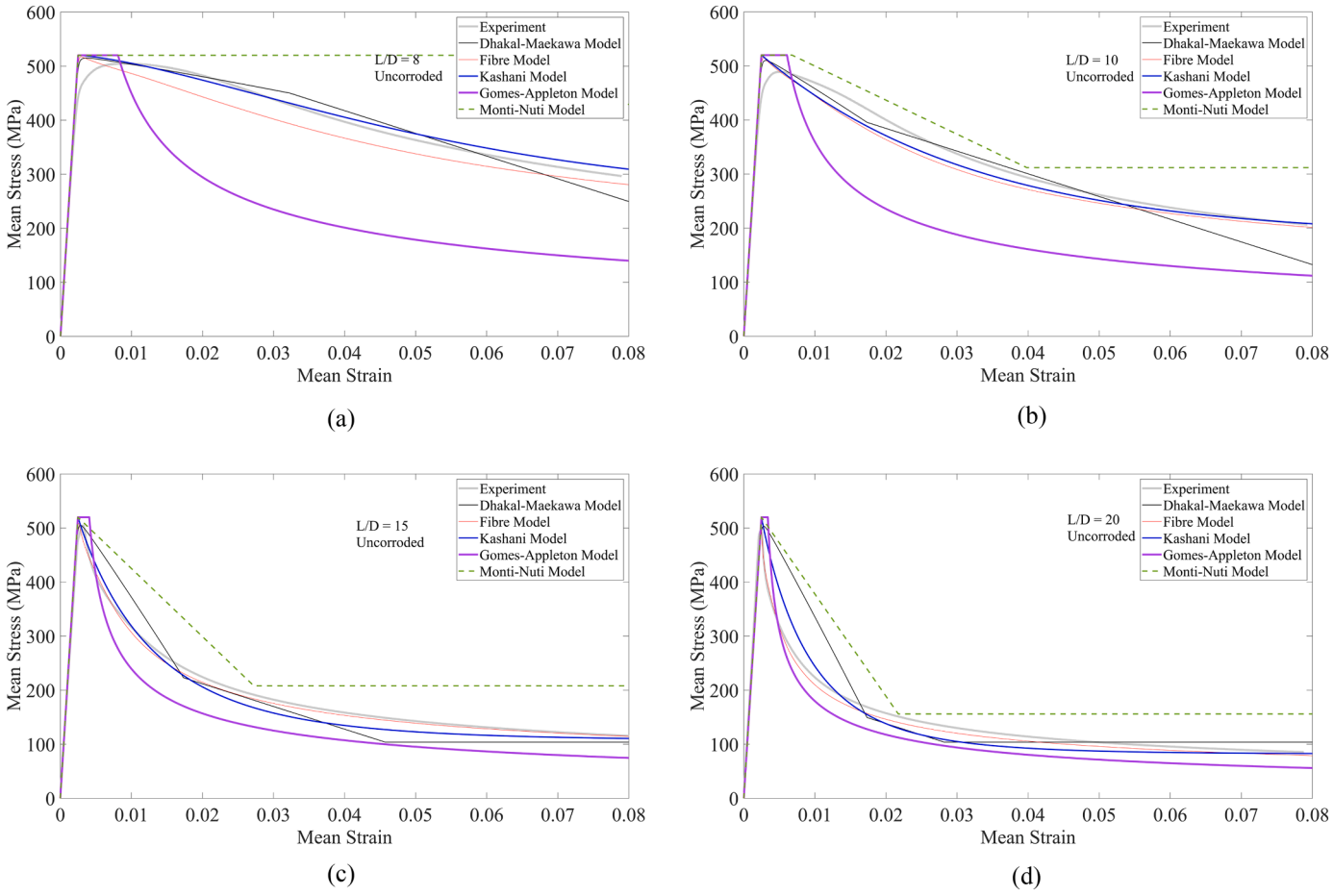

Fig. 1. Comparison of most widely used material models for post-buckling response of reinforcing bars: (a) $L/D = 8$, (b) $L/D = 10$, (c) $L/D = 15$, (d) $L/D = 20$.

induced mass loss.The compressive yield strength of corroded bars (σ'_{yc}) is estimated using the Eq. (15):

$$\sigma'_{yc} = \begin{cases} \sigma_y(1 - 0.005\ \psi) \text{for} L/D \le 6 \\ \sigma_y(1 - 0.0065\ \psi) \text{for} 6 < L/D < 10 \\ \sigma_y(1 - 0.0125\ \psi) \text{for} L/D \ge 10 \end{cases} \quad (15)$$

The proposed model for post-buckling response of corroded bars employs Eqs. (10) to (13) as discussed in Section 2.1.6 of this paper. The values of σ_y and D should be replaced with σ'_{yc} and D' in non-dimensional slenderness ratio, λ_p (Eq. (5)), and the minimum stress limit asymptotic, σ * (Eq. (12)).

2.2.2. Imperatore and Rinaldi model

Imperatore and Rinaldi [49] examined and discussed how uniform corrosion impacts the stress-strain behaviour of reinforcing bars when under monotonic compression loading through an extensive experimental testing programme. The study includes a broad range of specimens, each characterised by varying slenderness ratios (length-to-diameter ratios) and degrees of corrosion (experimental test parameters are available in Table A1 of this paper). The interaction between these factors and the overall response is thoroughly detailed. Ultimately, a simplified analytical model is formulated and presented, capable of capturing both peak stress and post-buckling behaviour. The formulation is following the approach developed by Gomes and Appleton [15] using three plastic hinge mechanisms (two at either ends of the bars and one in the middle). The analytical formulation yields to Eq. (15) to model the post-buckling response of corroded bars.

$$\sigma_N = \frac{8}{3\pi} \frac{\sigma_{y,cor,\lambda}}{\lambda_{cor}} \left(\frac{1}{\sqrt{1 - (\varepsilon_p - 1)^2}} \right) \quad (16)$$

where, $\lambda_{cor} = L/D'$, $\sigma_{y,corr,}\lambda$ is the compressive yield strength of corroded bars, and $\varepsilon_p = \varepsilon$ - ε_y is the plastic strain. The main difference between this model and Gomes and Appleton's model is that Eq. (16) reduces the yield strength in compression as a function of L/D ratio for uncorroded and corroded bars (D' for corroded bars).

$$\Delta\sigma_{y,\lambda} = 1 - \beta.\lambda_{corr} \quad (17)$$

where, $\beta = 0$ for $\lambda_{cor} \le 8$ and $\beta = 0.005$ for $\lambda_{cor} > 8$. Further details and derivation of Eqs. (16) and (17) are available in Imperatore and Rinaldi [49].

2.2.3. Comparison of the available post-buckling models for corroded reinforcing bars

Fig. 2 compares the only three available material models for simulating the post-buckling response of corroded bars against experimental data. The modified Dhakal-Maekawa and Kashani model are again in good agreement with experimental data. However, Imperatore-Rinaldi model, which follows the same assumption as Gomes-Appleton model underestimate the stress in bars with $L/D \le 10$. For the bars with L/D > 10 almost all three models show good agreement with the experimental data.

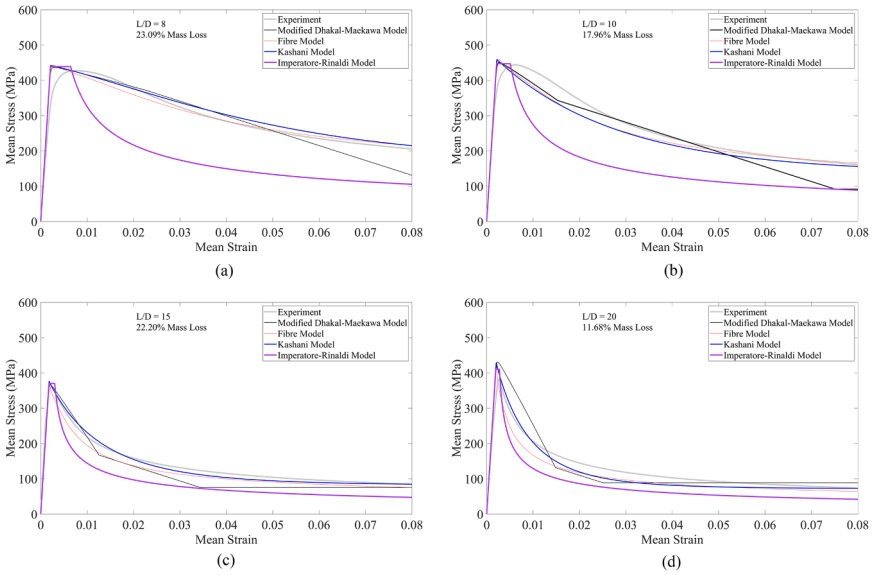

Fig. 2. Comparison of the available material models for post-buckling response corroded reinforcing bars: (a) L/D = 8% and 23.09% mass loss, (b) L/D = 10% and 17.96% mass loss, (c) L/D = 15% and 22.2% mass loss, (d) L/D = 20% and 11.68% mass loss.

3. Inelastic buckling of reinforcing bars under cyclic loading

3.1. Modelling nonlinear cyclic behaviour of reinforcing bars with the effect of inelastic buckling without corrosion

Table 2 shows a summary of previous studies on nonlinear cyclic response of reinforcing bars including inelastic buckling. The dataset extracted from a variety of literature sources comprises a large number of distinct reinforcing bar specimens. Similar to Table 1, these specimens were chosen to cover a range of scenarios. For additional information about the experimental dataset and all the associated parameters, you can refer to Table A1 in the appendix. Several researchers, as outlined in Table 2, have developed uniaxial material models that can be used in nonlinear finite element analysis of RC structures. Here the most widely used models and their parameters are presented, and a comparison between these models are provided.

3.1.1. Modelling nonlinear cyclic behaviour of reinforcing bars including the effect of buckling excluding low-cycle fatigue

Most of the previously proposed material models for the cyclic stress-strain behaviour of reinforcing bars employ variations of the original Menegotto–Pinto (MP) model [11]. Here, a summary of these models and their main features are provided.

Table 2
Previous studies on modelling inelastic buckling of reinforcing bars under cyclic loading.

Reference	Year of Study	Type of Study
Monti and Nuti[13]	1992	Experimental testing and uniaxial material model
Gomes and Appleton [15]	1997	Uniaxial material model
Rodriguez et al.[52]	1999	Experimental testing and uniaxial material model
Dhakal and Maekawa [17]	2002	Numerical and uniaxial material model
Prota et al.[16]	2009	Experimental testing and uniaxial material model
Kunnath et al.[18]	2009	uniaxial material model
Su et al.[53]	2015	Experimental testing and analytical modelling
Kashani et al.[46]	2015	Experimental testing and uniaxial material model
Yang et al.[54]	2016	uniaxial material model
Kim and Koutromanos [12]	2016	uniaxial material model

Monti and Nuti [13] have developed their models by making modifications to the Menegotto-Pinto model [11]. They introduced a set of guidelines based on experimental observations of how reinforcement bars buckle. While they adopted the stress-strain relationship from Menegotto-Pinto, they emphasized that other constitutive laws could be used as long as they are appropriately formulated. The Monti-Nuti model's parameters are vigorously adjusted after each load reversal. They employed two classical methods for this adjustment: (i) isotropic hardening, and (ii) kinematic hardening rules. Additionally, they incorporated (iii) a memory rule to account for the material's ability to "remember" the plastic path that it followed, and (iv) a saturation rule to accommodate the eventual levelling off of the hardening phenomena. These four rules were defined for both scenarios – with and without buckling. The buckling parameters are discussed in Section 2.1.1 of this paper, and further details about the cyclic rules can be found in Monti and Nuti [13].

Gomes and Appleton [15] undertook modifications to the Guiffre–Menegotto–Pinto model [11], resulting in the creation of a stress–-strain model that incorporates the impact of buckling. The Gomes and Appleton buckling model is discussed in Section 3.1.2 of this paper. Under cyclic loading, the Gomes–Appleton model directly follows the Guiffre–Menegotto–Pinto model in determining unloading path from tension and onset of buckling. This indicates that buckling is not included in the unloading path and reloading in tension. Further details can be found in Gomes–Appleton [15].

Rodriguez et al. [52] tested a series of reinforcing bars under monotonic cyclic loading. The tests were performed until the specimens failed, in all cases under compressive loading. To study the effects of the ratio of spacing of lateral supports (L) to bar diameter (D) on reinforcement stability, tests were performed for L/D ratios of 2.5, 4, 6, and 8. Using the experimental results, they proposed a procedure for predicting onset of buckling. It is shown that the initiation of buckling within a steel rebar, when exposed to hysteresis cycles, might occur during unloading from tension. This phenomenon exhibits a notable dependency on the peak value attained by the tensile strain before this reversal. Under these circumstances, the inception of buckling in a steel rebar could potentially take place within the tensile segment of the hysteresis cycle. Although this model can approximately predict the

onset of buckling under cyclic loading, the stress-strain response does not explicitly model the post-buckling response. Furthermore, the largest *L/D* tested in this study is 8, in which buckling has a relatively minor impact on the stress-strain response. Further details can be found in Rodriguez et al. [52].

Dhakal and Maekawa [17] presented a novel cyclic model for reinforcing bars, designed to rectify the limitations in previous models. Their model fulfils the subsequent criteria:

1) It systematically incorporates the influence of both geometrical and mechanical characteristics of the bar on its post-buckling behaviour. This applicability extends to bars characterized by diverse material properties and a variety of hardening mechanisms.
2) It follows to the $\sigma = f(\varepsilon)$ structure, a feature that confers notable benefits in any non-linear finite element (FE) computations based on kinematic approximations, such as displacement-controlled FE analysis.
3) Notably, it is fundamentally dependent on the deformation path, including all feasible strain histories.
4) This model is not only straightforward in formulation but also relies on material parameters that are readily obtainable. This facilitates effortless implementation and integration into any FE analysis program.

The buckling and post-buckling response of Dhakal and Maekawa's model is discussed in Section 2.1.4 of this paper. They employed Mander et al.'s [34]for tension envelope and Guiffre–Menegotto–Pinto model [11] for cyclic loading and unloading. They have made some modification to the Guiffre–Menegotto–Pinto model to account for inelastic buckling. Further details can be found in Dhakal and Maekawa [17].

Yang et al., 2016 [54] made adjustments to the cyclic steel stress–-strain relationship initially proposed by Gomes–Appleton [15]. These modifications aimed to enhance the precision of simulating the stress–strain path during inelastic buckling by utilising a simplified model based on the equilibrium of a plastic mechanism within a buckled bar, comprising four plastic hinges. Subsequently, they introduced an adjustment coefficient to further refine the buckled bar stress–strain model they developed. For the loading and unloading paths within the tension region of stress–strain curves, the Gomes–Appleton model had been following the Guiffre–Menegotto–Pinto model, which does not account for buckling effects. Consequently, the assumptions regarding the plastic hinges in the Gomes–Appleton model were revised from three to four, leading to the derivation of an average stress calculation formula for buckled reinforcing bars. The introduced adjustment coefficient aimed to rectify potential errors arising from deviations in the full plastic stress distribution assumption, particularly pertinent to small *L/D* ratios. The proposed model, demonstrated accurate simulation of unloading and reloading paths during tension-induced stress–strain behaviour in buckled reinforcing bars. To validate the model's efficacy, it was employed for numerical simulations of reversed cyclic tests of 41 specimens, including varied *L/D* ratios, yield strengths, and loading methodologies, as conducted by different researchers. A comparison between the simulation outcomes and experimental results showed the good accuracy and effectiveness of the proposed model. Further details are available in Yang et al., 2016 [54].

3.1.2. Modelling nonlinear cyclic behaviour of reinforcing bars including the effect of buckling and low-cycle fatigue

Many researchers have investigated the low-cycle fatigue life of reinforcing bars in the absence of buckling effects [55,56] [57]. These investigations have predominantly employed three approaches to characterise the low-cycle fatigue life of these bars: (*i*) Coffin-Manson model [58], (*ii*) Koh-Stephen model [59], and (*iii*) energy method [60]. It's worth noting that these models are specifically applicable to low-cycle fatigue occurring under conditions of constant amplitude loading. To address the cumulative damage resulting from random loading histories, Miner's rule [61] has been utilised (for a more detailed discussion, refer to [62]). Among the models mentioned above, the Coffin-Manson and Koh-Stephen models have gained prominence among researchers due to their simplicity in integration with various finite element software packages for seismic analysis of civil engineering structures. Both the Coffin-Manson and Koh-Stephen models adopt a strain-life approach for representing the low-cycle fatigue life of engineering materials. Within this framework, the plastic strain amplitude emerges as the most crucial parameter influencing the material's susceptibility to low-cycle fatigue. The fatigue life as a function of the plastic strain amplitude (ε_p) is described by Coffin-Manson in Eq. (16):

$$\varepsilon_p = \varepsilon'_f \left(2N_f\right)^c \tag{18}$$

where, ε'_f is the ductility coefficient i.e. the plastic fracture strain for a single load reversal, c is the ductility exponent and 2 N_f is the number of half-cycles (load reversals) to failure.Koh-Stephen [59] employed the Coffin-Manson for modelling the low-cycle fatigue life of materials based on the total strain amplitude (elastic strain + plastic strain) as shown in Eq. (17):

$$\varepsilon_a = \varepsilon_f \left(2N_f\right)^\alpha \tag{19}$$

where, ε_f is the ductility coefficient i.e. the total fracture strain for a single load reversal, α is the ductility exponent and *2 N_f* is the number of half-cycles (load reversals) to failure.

Kunnath et al., 2009 [18] developed a uniaxial material model relating equivalent strain and average stress, which implicitly includes the geometric effects of longitudinal bar buckling in a reinforced concrete section. Additionally, low-cycle fatigue failure and damage resulting from cyclic deterioration are also incorporated. The proposed model employed Chang and Mander model [60] for tension envelope, Dhakal and Maekawa buckling [38] for compression envelope, and Guiffre–Menegotto–Pinto model [11] for cyclic loading and unloading. Coffin-Manson [58] and Miner's rule [61] are used to model the low-cycle fatigue deration of reinforcing bars under cyclic loading. The simulation results showed a good agreement with experimental data. This refined constitutive material model for reinforcing bars is aimed to facilitate a more advanced representation of the cyclic degradation behaviour within RC structures. However, the influence of bar buckling on low-cycle fatigue degradation of reinforcing bars is not accounted in this model. This model is implemented to the OpenSees [4] (Material name in the OpenSees is *ReinforcingSteel*) and is available to be used by other researchers. The implemented model in the OpenSees has two options for buckling; i.e. Dhakal-Maekawa and Gomes-Appleton models.

Kim and Koutromanos in 2016 [12] introduced a uniaxial constitutive model for reinforcing steel that builds upon the model initially proposed by Dodd and Restrepo-Posada in 1995 [63]. This enhancement is achieved by eliminating the requirement for iterative processes during stress updates. The newly proposed material model includes considerations for both the initiation of local buckling and the subsequent post-buckling behaviour of reinforcing bars. Particularly, this model is endowed with the ability to incorporate the influences of low-cycle fatigue and the consequent rupture of reinforcing steel. A distinctive feature of this proposed material law is does not require number of cycles as the damage variable. Consequently, the need for employing a cycle-counting algorithm is obviated. Instead, the model operates on the premise that rupture transpires when a scalar damage variable, linked to the inelastic work accumulation under tensile stress, surpasses a critical threshold. Further details are available in Kim and Koutromanos 2016 [12]. Similar to Kunnath et al., 2009 [18], this model does not account for the influence of inelastic buckling on low-cycle fatigue degradation of reinforcing bars.

3.1.3. Comparison of the available nonlinear cyclic uniaxial material models including the effect of buckling

Fig. 3 shows a comparison between the *ReinforcingSteel* model in the OpenSess with two different buckling models which was implemented by Kunnath et al. [18], and Kashani model. Fig. 3(a) shows that there are large differences between the three models. These differences are due to the impact of inelastic buckling on cyclic response, which results in significant pinching in the stress-strain curves. Although the *ReinforcingSteel* includes two buckling models the formulation does not account for this pinching effect. This is because the model is not calibrated against bars with large *L/D* ratios and large strain amplitudes. Fig. 3(b) shows the comparison of Kashani model against experimental data. This shows that the model is able to capture the pinching response due to buckling. It should be noted that Kashani model includes low-cycle fatigue degradation too, which is discussed later in Section 3.2 of this paper.

Furthermore, *ReinforcingSteel* model shows numerical instability for large strain amplitudes (beyond ~3% strain), and therefore, it is not possible to compare this model with experimental data.

3.2. Modelling nonlinear cyclic behaviour of reinforcing bars including effect of inelastic buckling, corrosion damage, and low-cycle fatigue degradation

Kashani et al. [46] developed a new phenomenological hysteretic model that significantly improved the inelastic buckling simulation of reinforcing steel with and without corrosion damage. The main feathers of this model are:

i. It accounts for the combined effect of inelastic buckling and low-cycle fatigue.
ii. It accounts for the effect of corrosion damage on inelastic buckling and low-cycle fatigue life of reinforcing bars.
iii. It was calibrated against an extensive set of experimental and computational data.

The proposed model integrates both material nonlinearity and geometric nonlinearity arising from buckling, along with low-cycle fatigue degradation, into a unified material model. This model is currently the most advanced uniaxial material models, accurately tailored for reinforcing bars, which also accounts for corrosion damage.

Kashani et al. [51,64] conducted a series experimental testing and nonlinear finite element parametric study to investigate the nonlinear cyclic behaviour of uncorroded and corroded reinforcing bars. The simulations results showed that slenderness ratio of the bars known as the *L/D* ratio beyond 8 in reinforcing bars with yield strength between 400 MPa and 500 MPa results in a complex pinching effect in the hysteretic cycles. This is the result of geometrical nonlinearity on the cyclic response. Other researchers have also come up with the same conclusion based on the experimental results [49,65,66]. This demonstrates a consistent cyclic behaviour pattern in reinforcing bars influenced by buckling effects.

Kashani et al. [51] conducted a comparative analysis between the existing analytical models and computational results. They conclusively demonstrated that the pinching effect arising from geometric nonlinearity is absent in previous analytical models (e.g. *ReinforcingSteel* model in OpenSees). The pronounced pinching phenomenon within hysteretic cycles of longitudinal reinforcement plays a crucial role in the cyclic deterioration of RC components subjected to seismic loading. Consequently, its inclusion is imperative within the material modelling of reinforcement for nonlinear analysis of RC structures encountering cyclic loading. In this model the tension envelope utilises the model developed by Balan et al. [67], which constitutes a continuous function enabling a continuous shift from the linear elastic to the strain hardening zone. This enhancement will support the numerical stability in nonlinear finite element analyses. The corrosion in tension is modelled using the modification suggested by Du et al. [68,69] (further details are available in Kashani et al. [46]). The compression envelope to model the post-buckling response of bars including the effect of corrosion damage is discussed previously in Sections 2.15 and 2.2 of this paper.

This phenomenological model employs the fatigue life model in Eq. (17) and the methodology proposed by Kunnath et al. [18] to model low-cycle fatigue degradation of reinforcing bars under cycling loading. Kashani et al. [64,70] studied low-cycle fatigue life of reinforcing bars with the effect of corrosion using the available data in the literature. The analysis of the data showed that corrosion doesn't influence the material constant ε_f in Eq. (18). However, corrosion changes the material constant α. The relationship between corrosion and the material constant α, is described in Eq. (20) below:

$$\frac{\alpha_{corr}}{\alpha} = 1 + 0.004\,\psi \tag{20}$$

where, α_{corr} is the material constant of corroded bars. Accordingly the value of α in fatigue life model (Eq. (17)) can be replaced with α_{corr} to account for the influence of non-uniform pitting on fatigue life.

In another study Khashani et al. [62,71] investigated the influence of inelastic bucking on low-cycle fatigue life reinforcing bars. They proposed a set of empirical equations that modifies the fatigue life model of reinforcing bars a function of bar buckling parameter, λ_p (Eq. (5)) as describe below:

The relationship between the fatigue model parameters and λ_p is defined by empirical Eqs. (21) and (22):

$$\alpha = -0.017\,\lambda_p - 0.23 \tag{21}$$

$$\varepsilon_f = 0.053\,\exp(0.078\,\lambda_p) + 0.065 \tag{22}$$

The above equations have been implemented to the original model, and the updated model is currently the only available phenomenological

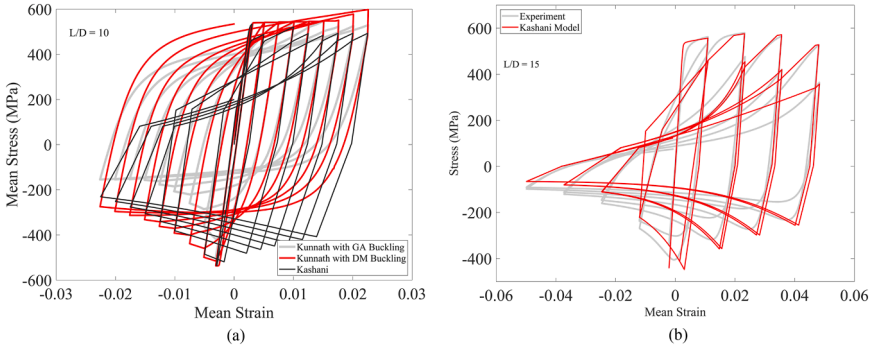

Fig. 3. Comparison of the available nonlinear cyclic material models with the effect of buckling: (a) three of the most common models (DM is Dhakal-Maekawa and GA is Gomes-Appleton), and (b) Kashani model and experimental data.

material model of reinforcing bars that accounts for inelastic buckling, corrosion damage, and influence of inelastic buckling on low-cycle fatigue life.

Fig. 4 shows a comparison between the Kashani and Kunnath (*ReinforcingSteel* in OpenSees) models and experimental data of a corroded bar. Here, the modified Dhakal-Maekawa model, as discussed in section 3.2.3 of this paper, in used in Kunnath model to account for corrosion and buckling. The comparison of the models and experimental data shows a good agreement between Kashani model experimental data. However, *ReinforcingSteel* cannot simulate the experimental results. Furthermore, as discussed earlier in section 4.1.3 of this paper, the *ReinforcingSteel* model in the OpenSees has numerical instability in large strain amplitudes (>~0.03), and therefore, it is not possible to compare this model across the whole hysteretic loops the observed experimental data.

4. Influence of tie reinforcement in global stability of longitudinal bars and buckling length calculation

The initial exploration of longitudinal reinforcement buckling within concrete columns was undertaken by Bresler and Gilbert [32]. They introduced an approach for estimating the critical load and buckling mode. This approach facilitated the design of lateral ties possessing the necessary rigidity to prevent bar buckling. In a parallel vein, Scribner [72] conducted an analytical study on bar buckling, employing an energy minimisation methodology similar to that used by Bresler and Gilbert. The findings revealed that employing ties exceeding the recommendations specified by seismic provisions, only proved effective in preventing certain modes of longitudinal reinforcement buckling in elements subjected to cyclic inelastic flexure.

Papia et al. [73] developed a model that utilised a positively symmetrical shape function to depict the buckled configuration of a longitudinal bar. They also accounted for the effects of longitudinal bar inelasticity during the buckling process by incorporating a reduced modulus. Employing an energy minimisation technique, they calculated the values of critical buckling load and critical buckling length.

Pantazopoulou [74] investigated the influence of tie reinforcement, limiting concrete strain in compression, bar diameter, and tie spacing on reinforcement stability in RC columns. To calculate this relationship, an extensive collection of data including more than 300 column tests was compiled from international literature sources. The tests incorporated within this collection were executed using repeated axial and flexural load reversals, aiming to replicate seismic forces on specimens featuring varied configurations of longitudinal and confining steel elements.

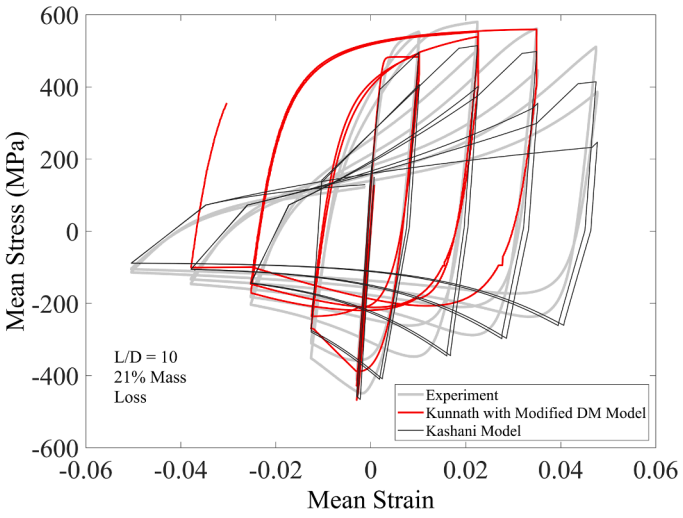

Fig. 4. Comparison of Kashani and Kunnath models with experimental data.

Subsequently, a systematic examination of the comprehensive dataset was conducted, seeking to determine from empirical observations the critical state at which reinforcement stability becomes acute. This critical stage was found to stand a direct correlation with factors such as the constrained average compressive strain and/or the demand for ductility in the plastic hinge region. Additionally, the geometry and effectiveness of confinement were integral considerations.

In 2002, Dhakal and Maekawa [39] introduced a straightforward and reliable approach for estimating both the buckling length of longitudinal reinforcing bars and the likelihood of concrete cover spalling in reinforced concrete components. Their methodology requires a comprehensive stability analysis that duly accounts for the geometric and mechanical properties of the longitudinal reinforcing bars and transverse ties. By employing energy principles, they established the necessary tie stiffness for protecting longitudinal reinforcing bars against multiple buckling modes. A comparison between this calculated tie stiffness and the actual value is then utilised to identify the mode of stable buckling. The actual buckling length is determined as the product of the stable buckling mode and the spacing between ties. To validate the efficacy of their proposed approach for buckling length determination, a range of cases is verified against experimental data available in the literature.

Massone and López 2014 [48] investigated the inelastic buckling behaviour of reinforcement under monotonic compression loading including the effects of tie reinforcement. They used the computational model that was originally developed by Massone and Moroder [43] for local buckling of reinforcing bars, assuming four plastic hinges. This model is modified to include the stiffness of tie reinforcement and core concrete expansion pressure over the buckling length of longitudinal bars. In contrast to many prior studies, the model presented in this research offers a unique feature, in addition to its ability to predict the buckling mode, it provides the stress–strain relationship for the buckled bars. This stress–strain curve can be effectively employed in both sectional and element analyses. Verification of the model against three column specimens sourced from existing literature, showed that while the exact representation of the buckling mode might not be achieved, a reasonable approximation of the overall stress versus strain behaviour can still be achieved. The peak stress in this model is predicted with an approximately 10% error relative to the experimental outcome, specifically for a strain level well captured by the model. Furthermore, the model provides a reliable estimate for the post-peak slope, which proves valuable in predicting the degradation stage.

Zong et al., 2014 [20] introduced a beam-on-springs model, applied to derive average stress-strain relationships for reinforcement bars within reinforced concrete columns of circular cross sections. The model parameters were determined through a systematic study that examined key factors influencing the buckling behaviour of longitudinal bars. Two versions of the model were presented: a general-purpose version and a simplified trilinear version designed for immediate use in existing nonlinear analysis software. The model effectively predicted the post-yield softening response attributed to buckling and verified through comparison with real-world observed behaviour. It should be noted that modelling and guidelines in this study are specific to columns with circular cross sections. Furthermore, the investigation into cyclic behaviour and degradation has not been pursued and should be explored in future research endeavours.

Su et al., 2015 [53] presented a simplified buckling model designed for columns with rectangular and circular cross sections. The model employed stability theory to predict buckling behaviour. To validate its effectiveness, six rectangular and five circular RC columns with varying reinforcement characteristics were subjected to consistent axial and reverse horizontal loads in experimental tests. The proposed simplified buckling model verified against experimental data, and its impact on the seismic behaviour of RC columns was explored. Through a comparative analysis of predicted and measured buckling lengths of longitudinal bars, the developed model was shown to accurately predict buckling

length of both rectangular and circular columns. The model indicated that several factors influenced the buckling length of longitudinal bars, including the shape of the column cross section, the arrangement of reinforcement, the elastic modulus of longitudinal bars, tie reinforcement spacing, diameter of longitudinal bars, and tie reinforcement diameter. The outcomes of this study suggest that the stiffness of tie reinforcement is more pronounced in circular cross sections than in rectangular ones. Consequently, longitudinal bars in circular columns exhibited a shorter buckling length, contributing to larger hysteresis loops in circular columns. Circular columns also showed more ductility and energy dissipation capacity compared to their rectangular counterparts. Furthermore, the yield strength of tie reinforcement had minimal impact on the buckling of longitudinal bars. Consequently, under low axial loads, the primary failure mode of RC columns is govern by longitudinal bar buckling, and high-strength tie reinforcement had almost no effect on the seismic performance of RC columns.

Vecchi and Belletti [75] made some modifications to the original Kashani model [46] to account for the influence of tie stiffness on average stress-strain behaviour of reinforcing bars in compression. These modifications was based on experimental observations and a numerical parametric study [76,77] [78,79]. The proposed model was successfully implemented in ABAQUS (embedded reinforcement using truss element) and verified against experimental data. However, these modifications are not based on mechanics, and hence, they need further verification before they can be used by other researchers.

5. Design guidelines for buckling length calculations and anti-buckling tie reinforcement

In 2018, Dhakal and Su [80] introduced a new design criterion aimed at mitigating buckling effects. This criterion draws from a widely accepted bar buckling model [38,39], utilising a parameter combining bar diameter, yield strength, and buckling length to characterise bar buckling behaviour. The specified buckling parameter, which limits buckling-induced stress loss to a about 15% in compression bars at the strain corresponding to design ductility, is determined. By establishing this value, the maximum allowable buckling length for a given bar diameter and yield strength can be estimated. This length in turn establishes an upper boundary for spacing between transverse ties or hoops. The stiffness required to stabilise main bar buckling near the positions of transverse ties or hoops is depending on the flexural rigidity of the main bars and the buckling length, which can match or be multiples of the spacing between transverse ties or hoops. On the other hand, the efficacy of transverse reinforcement in preventing buckling depends on their dimensions, quantity, and arrangement. Building on this concept, practical design guidelines are formulated for the quantity, layout, and spacing of rectangular and circular ties. These guidelines ensure that the anti-buckling capacity of the provided transverse reinforcement surpasses the restraint required to minimise the vulnerability of main bars to buckling. Validation of key elements within this method was performed through experimental tests available in the literature. They have also reviewed the anti-buckling detailing rules in the current seismic design codes, and confirmed that the criteria for spacing between the ties or hoops are acceptable. However, none of the current seismic design codes account for the stiffness of time or hoop reinforcement. Therefore, they suggested the following steps that enhances the current design procedure. Further details and derivation of the equations are available in Dhakal and Su [80].

Step 1: Design of transverse reinforcement for shear and confinement.

Step 2: Calculate the buckling length:

$$\text{Full ductility}: L = 14\frac{D}{\sqrt{\sigma_y/100}} \tag{23}$$

$$\text{Limited ductility}: L = 18\frac{D}{\sqrt{\sigma_y/100}} \tag{24}$$

Step 3: Check if the spacing of ties, $s \leq$ buckling length, L in Eq.s (21) and (22), If not assume $s = L$Step 4: Calculate the required stiffness of ties, K_t, to prevent buckling as a function of flexural rigidity of longitudinal reinforcement:

$$K_t = 0.75\frac{\pi^4 EI_{eff}}{s^3}; EI_{eff} = \frac{EI}{2}\sqrt{\frac{\sigma_y}{400}} \tag{25}$$

where E, I, and σ_y are the elastic modulus, second moment of area, and yield strength of vertical bars respectively.Step 5: Calculate the stiffness of tie for the specific cross section:

$$\text{For rectangular sections}: K_r = \frac{E_t A_t}{n_b}\sum_{i=1}^{n_l}\frac{\cos^2\theta_i}{l_{tie}} \tag{26}$$

where E_t and A_t are elastic modulus and cross section area of each transverse tie leg, n_b is the number of longitudinal bars on the side of the section that is prone to buckling, n_l is the total number of legs provide by transverse reinforcement; θ_i is the angle between the side of the buckling face of the section and leg of tie reinforcement, and l_{tie} is length of tie leg for the i_{th} leg. The values of n_b, n_l, l_{tie}, and θ_i for some common arrangements of main bars and lateral ties in square/rectangular cross sections are provided in Dhakal and Su [80].

$$\text{For circular sections}: K_c = \frac{E_t A_t}{D}\frac{1}{n_b} \tag{27}$$

$$n_b = 1 + 2\left[\frac{n_t}{2\pi}\cos^{-1}\left(1 - 2\frac{D}{D_c}\right)\right]_{\text{integer}} \tag{28}$$

where D is the diameter of longitudinal bars, and D_c is the diameter of the RC section.

Step 6: Check if K_r or $K_c \geq K_t$, if not, repeat the Step 5 until this condition is satisfied.

5.1. Influence of corrosion on anti-buckling tie reinforcement

Kashani et al. [81] developed a set of probabilistic model using a lognormal distribution for calculation of geometrical properties of corroded bars. Here, the mean value of the lognormal distribution models can be used to model the effect of pitting corrosion on the geometric properties of corroded bars. Further details and derivation of these equations are available in Kashani et al. [81].

The Eq. (29) can be used to calculate the average reduced cross section area, A_{ave}, of reinforcement considering a linear reduction in area as function of percentage mass loss ψ.

$$A_{ave} = A_0(1 - 0.01\,\psi) \tag{29}$$

where, A_0 is the corresponding original uncorroded cross section area. The cross section area allowing for pitting effect (A') can be calculated using the Eq. (30).

$$A' = \Upsilon\, A_{ave} \tag{30}$$

where, Υ is the mean value of area pitting coefficient.The minimum second moment of area of corroded bars ($I'_{\min}$) can be calculated by introducing a pitting coefficient for second moment of area as defined in Eq. (31) below:

$$I'_{\min} = K\, I_0 \tag{31}$$

where, K is the mean value of pitting coefficient of minimum second moment of area of the corroded bars, and I_0 is the second moment of corresponding the uncorroded bar.The mean values of the pitting

coefficients (ϒ and K) can be calculated using the Eq. (32).

$$M_{(\Upsilon or K)} = \exp\left(\mu + \frac{\sigma^2}{2}\right) \quad (32)$$

where, μ and σ are defined in Eqs. (33) and (34) below:

$$\mu = a\,\psi^b \quad (33)$$

$$\sigma = c\,\psi^d \quad (34)$$

The values of coefficients a, b, c and d are provided in Table 3 below. Finally, the values of σ_y, D, I, and A_t should be replaced with σ'_{yc} (Eq. (15)), D' (Eq. (14)), A' (Eq. (30)), and I'_{min} (Eq. (31)) in Eqs. (23) to (28).

6. Unresolved issues and future research needs

Although there are several inelastic buckling models available in the literature, there is still no reliable and stable model readily available that can simulate the nonlinear cyclic response of RC elements. Currently OpenSees and SeismoStruct [4,5] are the most widely used fibre-based finite element platforms that have uniaxial material models for reinforcing bars accounting for buckling. However, these models are not numerically stable, and cannot be easily used in the nonlinear seismic analyses of RC components. Furthermore, almost all of the available models have been developed and calibrated using numerical and experimental data of bare reinforcing bars rather than average stress-strain behaviour of bars in RC elements. Kashani et al. [77,78] calibrated their models for circular and rectangular RC columns, but this model is calibrated empirically against experimental data. This is because the influence of tie stiffness on average stress-strain response of buckled bar under monotonic and cyclic loading should be considered in the material model, which is different for circular and rectangular sections. As discussed in Section 4 of this paper, several researchers have attempted to address this issue but there is still no model readily available that accounts for such interaction.

Influence of tension strain on the onset of inelastic buckling of bars is another important parameters that affects the performance of RC components under seismic loading. Depending on the strain history, the onset of buckling is different. Some of the researchers [82,83] have attempted to address this issue, but there is still no model available in the literature that is able to capture the influence of tension strain history on the onset of buckling.

This is mainly because the onset of buckling of longitudinal bars inside concrete (at about 0.002 strain for bars with $L/D>8$) is occurring prior to the spalling of concrete cover (at about 0.004 strain), and hence, it is invisible. Since inelastic buckling of vertical bars is a combined material and geometrical nonlinear problem, internal strain gauges cannot be used to identify the onset of buckling. Furthermore, as mentioned above, inelastic buckling is a load path dependent phenomenon. The experimental tests can only capture limited cyclic load histories, and hence, the path dependency cannot be easily capure in experimental data. As a results, the only approach that can be used in simulation of inelastic buckling of longitudinal bars inside concrete is high-fidelity 3D continuum finite element models such as those reported in [20].

The abovementioned issues are related to uncrroded reinforcing bars. The same issues are valid for corroded reinforcing bars, and presence of pitting corrosion makes these issues much more complicated to solve. Furthermore, the influence of localised pitting corrosion of tie reinforcement on stability and buckling length of longitudinal reinforcement is yet to be addressed. This is very important parameter, which is different for circular and rectangular section. The chloride penetration in circular columns is almost uniform in all the bars, however, in rectangular columns the corner bars are subjected to two-dimensional chloride penetration from two sides. The two-dimensional chloride penetration in corner bars in rectangular sections results in more severe corrosion in longitudinal and tie reinforcement [84], and hence, they are more vulnerable to buckling. Therefore there is a need for further research in corroded RC components to investigate this phenomenon in more detail.

Table 3
Probabilistic model parameters in Eqs. (31) and (32).

Model Parameter	*a*	*b*	*c*	*d*
ϒ				
μ	-0.000052	1.825		
σ			0.0006491	1.526
K				
μ	-0.008811	1.354		
σ			0.001768	1.495

7. Conclusions

This paper presents a comprehensive review of all the available (most widely used) uniaxial material models of reinforcing bars including the effects of buckling under monotonic and cyclic loading. A comparison between various models and experimental data is presented and a critical review on the ability of each model to simulate the nonlinear behaviour of reinforcing bars under monotonic and cyclic loading is provided. The main outcomes of this state-of-the-art review paper can be summarised as follows:

(1) The existing models can simulate the nonlinear stress-strain behaviour of reinforcing bars under monotonic cyclic loading including inelastic buckling. However, there is a need for significant model calibration for such models to be able to use them in simulating the nonlinear seismic behaviour of RC components.
(2) There is a need for further research to account for the influence of transverse tie reinforcement on the average cyclic stress-strain behaviour of longitudinal bars after onset of buckling (pinching response).
(3) The specific anti-buckling rules in the current seismic design codes do not account for the stiffness of tie reinforcement. The simplified rules provided in Section 5 can be used to improve the current design practice.
(4) The impact of pitting corrosion on nonlinear stress-strain behaviour of reinforcing bars in compression and cyclic loading needs further research. The location of pitted section along the bar has significant impact on the nonlinear cyclic response of corroded bars.
(5) The impact of inelastic buckling on low-cycle fatigue failure of reinforcing bars need further refinement. The existing fatigue models are all based on experimental tests of bare reinforcing bars. As mentioned in conclusion (2), the average stress-strain response of reinforcing bars in concrete is affected by the stiffness of tie reinforcement. This has a significant impact on low-cycle fatigue degradation of longitudinal reinforcing bars, and hence, it requires further research.
(6) The impact of corrosion on low-cycle fatigue failure of reinforcing bars with and without the effect of buckling needs further research. In this context, the bar diameter is very important as it might affect the pitting corrosion pattern as well as low-cycle fatigue life.
(7) The conclusion (2) to (4) are applicable to corroded reinforcing bars and RC component too. However, pitting corrosion makes these issues much more complicated, and hence, further extensive experimental testing is required to investigate these issues.
(8) This review paper is limited to simulating inelastic buckling of reinforcing bars under monotonic compression and cyclic loading including low-cycle fatigue (with and without the present of corrosion damage). There is a need for a similar paper to compare their performance of these models when they are implemented in

RC structural components. Nevertheless, this paper provides a comprehensive guidance to other researchers for future research.

Declaration of Competing Interest

The authors declare that they have no known competing financial interests or personal relationships that could have appeared to influence the work reported in this paper.

Data Availability

No data was used for the research described in the article.

Appendix A

Table A1
Experimental test data and parameters.

Reference	Year of Study	Number of Specimens	Loading	D (mm)	L/D	σ_y (MPa)	ε_y	$\varepsilon_{sh}/\varepsilon_y$	$\varepsilon_u/\varepsilon_y$	σ_u/σ_y
Mander et al.	1984	3 uncorroded	Monotonic	16	6,10,15	295	0.00148	16.90	129.00	1.47
Monti and Nuti [13]	1992	3 uncorroded	Monotonic	16	5,8,11	440	0.0024	1.00	16.00	1.40
Monti and Nuti [13]	1992	3 uncorroded	Monotonic	20	5,8,11	440	0.0024	1.00	16.00	1.40
Monti and Nuti [13]	1992	3 uncorroded	Monotonic	24	5,8,11	440	0.0024	1.00	16.00	1.40
Monti and Nuti [13]	1992	3 uncorroded	Cyclic	16	5, 11	440	0.0024	2.90	29.20	1.29
Monti and Nuti [13]	1992	3 uncorroded	Cyclic	20	5, 11	440	0.0024	2.90	29.20	1.29
Monti and Nuti [13]	1992	3 uncorroded	Cyclic	24	5, 11	440	0.0024	2.90	29.20	1.29
Rodriguez et al. [52]	1999	10 uncorroded	Monotonic	16 (machined from 32 mm bars)	2.5,4,6,8	449	0.0022	4.05	54.55	1.86
Rodriguez et al. [52]	1999	26 uncorroded	Cyclic	16 (machined from 32 mm bars)	2.5,4,6,8	449	0.0022	4.05	54.55	1.86
Bayrak and Sheikh [37]	2001	7 uncorroded	Monotonic	20	4,5,6,7,8,9,10	520	0.0026	3.80	57.70	1.34
Bae et al.[40]	2005	9 uncorroded	Monotonic	25	4,5,6,7,8,9,10,11,12	437	0.0022	4.20	66.80	1.67
Bae et al.[40]	2005	9 uncorroded	Monotonic	32	4,5,6,7,8,9,10,11,12	444	0.0022	4.10	71.80	1.44
Cosenza and Prota [41]	2006	3 uncorroded (smooth bars)	Monotonic	8	5 to 70	358	0.0018	20.56	119.44	1.25
Cosenza and Prota [41]	2006	3 uncorroded (smooth bars)	Monotonic	12	5 to 70	327	0.0016	20.00	144.38	1.34
Cosenza and Prota [41]	2006	3 uncorroded (smooth bars)	Monotonic	14	5 to 70	351.5	0.0021	11.43	107.14	1.26
Cosenza and Prota [41]	2006	3 uncorroded (smooth bars)	Monotonic	16	5 to 70	321	0.0016	18.75	138.75	1.32
Prota et al.[16]	2009	1 uncorroded (smooth bars)	Cyclic	8	5 to 15,20,25,50,75,100	358	0.0018	20.56	119.44	1.25
Prota et al.[16]	2009	1 uncorroded (smooth bars)	Cyclic	12	6 to 15,20,25,50,75,100	327	0.0016	20.00	144.38	1.34
Prota et al.[16]	2009	1 uncorroded (smooth bars)	Cyclic	14	7 to 15,20,25,50,75,100	351.5	0.0021	11.43	107.14	1.26
Prota et al.[16]	2009	1 uncorroded (smooth bars)	Cyclic	16	8 to 15,20,25,50,75,100	321	0.0016	18.75	138.75	1.32
Kashani et al.[45]	2013	5 uncorroded and 42 corroded	Monotonic	12	5,8,10,15,20	520	0.00247	-	24.42	1.18
Kashani et al.[45]	2013	3 uncorroded and 40 corroded	Cyclic	12	5,10,15	520	0.00247	-	24.42	1.18
Kashani et al.[46]	2015	30 uncorroded	Low-Cycle Fatigue	12	5, 8, 10, 12,15	535	0.00281	10.21	50.89	1.18
Kashani et al.[46]	2015	30 uncorroded	Low-Cycle Fatigue	16	5, 8, 10, 12,15	544	0.00271	6.75	38.38	1.18
Kashani et al.[46]	2015	12 uncorroded and 48 corroded	Low-Cycle Fatigue	12	5,10,15	535	0.00281	10.21	50.89	1.18
Kashani et al.[50]	2017	6 uncorroded and 5 corroded	Monotonic	10	5, 8, 10, 12, 15,20	538	0.00269	12.01	56.80	1.17
Kashani et al.[50]	2017	6 uncorroded and 10 corroded	Monotonic	12	5, 8, 10, 12, 15,20	540	0.00268	11.47	54.03	1.19
Kashani et al.[50]	2017	6 uncorroded and 6 corroded	Monotonic	16	5, 8, 10, 12, 15,20	530	0.00273	9.33	60.37	1.21
Kashani et al.[50]	2017	6 uncorroded and 7 corroded	Monotonic	20	5, 8, 10, 12, 15,20	530	0.00258	9.02	55.66	1.19
Imperatore and Rinaldi[49]	2019	10 uncorroded and 36 corroded	Monotonic	16	5, 8, 10,15,20	520	0.00272	9.34	51.47	1.19
Kashani et al.[71]	2019	30 uncorroded	Low-Cycle Fatigue	10	5, 8, 10, 12, 15	538	0.00269	12.01	56.80	1.17
Kashani et al.[71]	2019	30 uncorroded	Low-Cycle Fatigue	12	5, 8, 10, 12, 15	540	0.00268	11.47	54.03	1.19

(continued on next page)

Table A1 (*continued*)

Reference	Year of Study	Number of Specimens	Loading	D (mm)	L/D	σ_y (MPa)	ε_y	ε_{sh} $/\varepsilon_y$	ε_u $/\varepsilon_y$	$\sigma_u/$ σ_y
Kashani et al.[71]	2019	30 uncorroded	Low-Cycle Fatigue	16	5, 8, 10, 12, 15	530	0.00273	9.33	60.37	1.21
Kashani et al.[71]	2019	30 uncorroded	Low-Cycle Fatigue	20	5, 8, 10, 12, 15	530	0.00258	9.02	55.66	1.19

σ_y = yield sress, σ_u = ultimate sress, ε_y = yield strain, ε_u = strain at ultimate stress, ε_{sh} = strain at strain hardening point.

References

[1] E. Spacone, F.C. Filippou'and, F.F. Taucer', Fibre beam-column model for non-linear analysis of r/c frames: part I. formulation vol. 25 (1996).
[2] E. Spacone, F.C. Filippou'and, F.F. Taucer', Fibre beam-column model for non-linear analysis o f r/c frames: part II. applications vol. 25 (1996).
[3] Pugh J. Numerical Simulation of Walls and Seismic Design Recommendations for Walled Buildings. PhD Thesis. University of Washington, 2013.
[4] Pacific Earthquake Engineering Research Centre. OpenSees The Open System for Earthquake Engineering Simulation 2023.
[5] Earthquake Engineering Software Solutions. Seismosoft 2023.
[6] Computers and Structures Inc. SAP2000 Structural analysis and design software 2023.
[7] M.P. Berry, M.O. Eberhard, Perform. Model. Strateg. Mod. Reinf. Concr. Bridge Columns (2008).
[8] M.P. Berry, M.O. Eberhard, Practical performance model for bar buckling, J. Struct. Eng. 131 (2005) 1060–1070.
[9] M.P. Berry, D.E. Lehman, L.N. Lowes, Lumped-plasticity models for performance simulation of bridge columns, Acids Struct. J. 105 (2008) 270–279.
[10] Moehle J.P., Lehman D.E. Seismic Performance of Confined Concrete Bridge Columns n.d.:23–42.
[11] M. Menegotto, P.E. Pinto, Method of analysis for cyclically loaded RC plane frames including changes in geometry and non-elastic behavior of elements under combined normal force and bending, Proc. IABSE Symp. . Resist. Ultim. Deform Abil. Struct. Acted Well Defin. Repeated Loads (1973) 15–22.
[12] S.H. Kim, I. Koutromanos, Constitutive model for reinforcing steel under cyclic loading, J. Struct. Eng. 142 (2016), https://doi.org/10.1061/(asce)st.1943-541x.0001593.
[13] G. Monti, C. Nuti, Nonlinear cyclic behavior of reinforcing bars including buckling, J. Struct. Eng. 118 (1992) 3268–3284.
[14] H. Nakamura, TH, Modelling of nonlinear cyclic behaviour of reinforcing bars, Acids Spec. Publ. 205 (2002) 273, https://doi.org/10.14359/11644.
[15] A. Gomes, J. Appleton, Nonlinear cyclic stress-strain relationship of reinforcing bars including buckling vol. 19 (1997).
[16] A. Prota, F. De Cicco, E. Cosenza, Cyclic behavior of smooth steel reinforcing bars: experimental analysis and modeling issues, J. Earthq. Eng. 13 (2009) 500–519, https://doi.org/10.1080/13632460902837686.
[17] R.P. Dhakal, K. Maekawa, Path-dependent cyclic stress-strain relationship of reinforcing bar including buckling vol. 24 (2002).
[18] S.K. Kunnath, Y. Heo, J.F. Mohle, Nonlinear uniaxial material model for reinforcing steel bars, J. Struct. Eng. 135 (2009) 335–343.
[19] M.S. Hoehler, J.F. Stanton, Simple phenomenological model for reinforcing steel under arbitrary load, J. Struct. Eng. 132 (2006) 1061–1069.
[20] Z. Zong, S. Kunnath, G. Monti, Material model incorporating buckling of reinforcing bars in RC columns, J. Struct. Eng. 140 (2014), https://doi.org/10.1061/(asce)st.1943-541x.0000808.
[21] F. Di Carlo, A. Meda, Z. Rinaldi, Numerical evaluation of the corrosion influence on the cyclic behaviour of RC columns, Eng. Struct. 153 (2017) 264–269, https://doi.org/10.1016/j.engstruct.2017.10.020.
[22] A. Meda, S. Mostosi, Z. Rinaldi, P. Riva, Experimental evaluation of the corrosion influence on the cyclic behaviour of RC columns, Eng. Struct. 76 (2014) 112–123, https://doi.org/10.1016/j.engstruct.2014.06.043.
[23] Z. Rinaldi, F. Di Carlo, S. Spagnuolo, A. Meda, Influence of localised corrosion on the cyclic response of reinforced concrete columns, Eng. Struct. 256 (2022), https://doi.org/10.1016/j.engstruct.2022.114037.
[24] E. Afsar Dizaj, M.M. Kashani, Nonlinear structural performance and seismic fragility of corroded reinforced concrete structures: modelling guidelines, Eur. J. Environ. Civ. Eng. 26 (2022) 5374–5403, https://doi.org/10.1080/19648189.2021.1896582.
[25] E. Afsar Dizaj, M.M. Kashani, Numerical investigation of the influence of cross-sectional shape and corrosion damage on failure mechanisms of RC bridge piers under earthquake loading, Bull. Earthq. Eng. 18 (2020) 4939–4961, https://doi.org/10.1007/s10518-020-00883-3.
[26] E. Afsar Dizaj, R. Madandoust, M.M. Kashani, Exploring the impact of chloride-induced corrosion on seismic damage limit states and residual capacity of reinforced concrete structures, Struct. Infrastruct. Eng. (2017), https://doi.org/10.1080/15732479.2017.1359631.
[27] M.M. Kashani, J. Maddocks, E.A. Dizaj, Residual capacity of corroded reinforced concrete bridge components: state-of-the-art review, J. Bridge Eng. 24 (2019), https://doi.org/10.1061/(asce)be.1943-5592.0001429.
[28] E. Afsar Dizaj, M.R. Salami, M.M. Kashani, Seismic vulnerability assessment of ageing reinforced concrete structures under real mainshock-aftershock ground motions, Struct. Infrastruct. Eng. 18 (2022) 1674–1690, https://doi.org/10.1080/15732479.2021.1919148.
[29] E.A. Dizaj, J.E. Padgett, M.M. Kashani, A Markov chain-based model for structural vulnerability assessmentof corrosion-damaged reinforced concrete bridges, Philos. Trans. R. Soc. A: Math., Phys. Eng. Sci. 379 (2021), https://doi.org/10.1098/rsta.2020.0290.
[30] F.R. Shanley, Applied column theory, Am. Soc. Civ. Eng. 115 (1950) 698–727.
[31] F.R. Shanley, Inelastic column theory, J. Aero¬nautical Sci. 14 (1947) 261–268.
[32] B. Bresler, H. Gilbert, Tie requirements for reinforced concrete columns, J. Am. Concr. Inst. 58 (1961) 555–569.
[33] Johnston B.G. Behaviour of Inelastic Buckling Model between the Tangent Modulus and Shanley Loads n.d.
[34] J.B. Mander, M.J.N. Priestley, R. Park, Seismic Design of Bridge Piers, Research Report 84-2, Christchurch, New Zealand, 1984.
[35] S.T. Mau, M. El-Mabsout, Inelastic buckling of reinforcing bars, J. Eng. Mech. 115 (1989) 1–17.
[36] M. Papia, G. Russo, Compressive concrete strain at buckling of longitudinal reinforcement, J. Struct. Eng. 115 (1989) 382–397.
[37] O. Bayrak, S.A. Sheikh, Plastic hinge analysis, J. Struct. Eng. 127 (2001) 1092–1100. –100.
[38] R.P. Dhakal, K. Maekawa, Modeling for postyield buckling of reinforcement, J. Struct. Eng. 128 (2002) 1139–1147, https://doi.org/10.1061/ASCE0733-94452002128:91139.
[39] R.P. Dhakal, K. Maekawa, Reinforcement stability and fracture of cover concrete in reinforced concrete members, J. Struct. Eng. 128 (2002) 1253–1262.
[40] S. Bae, A.M. Mieses, O. Bayrak, Inelastic buckling of reinforcing bars, J. Struct. Eng. 131 (2005) 314, https://doi.org/10.1061/(asce)0733-9445(2005)131:2(314).
[41] E. Cosenza, A. Prota, Experimental behaviour and numerical modelling of smooth steel bars under compression vol. 10 (2006).
[42] L.M. Gil-Martín, E. Hernández-Montes, M. Aschheim, S.J. Pantazopoulou, Approximate expressions for the simulated response of slender longitudinal reinforcement in monotonic compression, Mag. Concr. Res. 60 (2008) 391–397, https://doi.org/10.1680/macr.2006.00004.
[43] L.M. Massone, D. Moroder, Buckling modeling of reinforcing bars with imperfections, Eng. Struct. 31 (2009) 758–767, https://doi.org/10.1016/j.engstruct.2008.11.019.
[44] C.R. Urmson, J.B. Mander, Local buckling analysis of longitudinal reinforcing bars, J. Struct. Eng. 138 (2012) 62–71, https://doi.org/10.1061/(asce)st.1943-541x.0000414.
[45] M.M. Kashani, A.J. Crewe, N.A. Alexander, Nonlinear stress-strain behaviour of corrosion-damaged reinforcing bars including inelastic buckling, Eng. Struct. 48 (2013) 417–429, https://doi.org/10.1016/j.engstruct.2012.09.034.
[46] M.M. Kashani, L.N. Lowes, A.J. Crewe, N.A. Alexander, Phenomenological hysteretic model for corroded reinforcing bars including inelastic buckling and low-cycle fatigue degradation, Comput. Struct. 156 (2015) 58–71, https://doi.org/10.1016/j.compstruc.2015.04.005.
[47] Zong Z. Uniaxial Material Model Incorporating Buckling for Reinforcing Bars in Concrete Structures Subjected to Seismic Loads. PhD Thesis, University of California Davis, 2010.
[48] L.M. Massone, E.E. López, Modeling of reinforcement global buckling in RC elements, Eng. Struct. 59 (2014) 484–494, https://doi.org/10.1016/j.engstruct.2013.11.015.
[49] S. Imperatore, Z. Rinaldi, Experimental behavior and analytical modeling of corroded steel rebars under compression, Constr. Build. Mater. 226 (2019) 126–138, https://doi.org/10.1016/j.conbuildmat.2019.07.109.
[50] M.M. Kashani, Size effect on inelastic buckling behavior of accelerated pitted corroded bars in porous media, J. Mater. Civ. Eng. 29 (2017), https://doi.org/10.1061/(ASCE)MT.1943-5533.0001853.
[51] M.M. Kashani, L.N. Lowes, A.J. Crewe, N.A. Alexander, Finite element investigation of the influence of corrosion pattern on inelastic buckling and cyclic response of corroded reinforcing bars, Eng. Struct. 75 (2014) 113–125, https://doi.org/10.1016/j.engstruct.2014.05.026.
[52] Mario Rodriguez B.E., Botero J.C., Villa J. Cyclic stress-strain behavior of reinforcing steel including effect of buckling. n.d.
[53] J. Su, J. Wang, Z. Bai, W. Wang, D. Zhao, Influence of reinforcement buckling on the seismic performance of reinforced concrete columns, Eng. Struct. 103 (2015) 174–188, https://doi.org/10.1016/j.engstruct.2015.09.007.
[54] H. Yang, Y. Wu, P. Mo, J. Chen, Improved nonlinear cyclic stress-strain model for reinforcing bars including buckling effect and experimental verification, Int. J. Struct. Stab. Dyn. 16 (2016), https://doi.org/10.1142/S0219455416400058.
[55] J.B. Mander, F.D. Panthaki, A. Kasalanatp, Low-cycle fatigue behavior of reinforcing steel, J. Mater. Civ. Eng. 6 (1993) 453–468.

[56] Brown J., Kunnath S.K. Low-Cycle Fatigue Behavior of Longitudinal Reinforcement in Reinforced Concrete Bridge Columns. 2000.
[57] T. Higai, H. Nakamura, S. Saito, Fatigue failure criterion for deformed bars subjected to large deformation reversals, Acids Spec. Publ. 237 (2006) 37–54, https://doi.org/10.14359/18244.
[58] S.S. Manson, Fatigue: a complex subject-some simple approximations - both ends of the fatigue spectrum are covered in this lecture. On the one hand, the present state of understanding of the mechanism is reviewed and the complexity of the process observed. On the other hand, some approximations useful in design are outlined and their application illustrated, Exp. Mech. 5 (1965), https://doi.org/10.1007/BF02321056.
[59] S.K. Koh, R.I. Stephens, Mean stress effects on low cycle fatigue for a high strength steel, Fatigue Fract. Eng. Mater. Struct. 14 (1991), https://doi.org/10.1111/j.1460-2695.1991.tb00672.x.
[60] Chang G., Mander J.B. Seismic energy based fatique damage analysis of bridge columns - part I - evaluation of seismic capacity. Technical Report NCEER-94–0006 1994.
[61] M.A. Miner, Cumulative damage in fatigue, J. Appl. Mech., Trans. ASME vol. 12 (1945), https://doi.org/10.1115/1.4009458.
[62] M.M. Kashani, A.K. Barmi, V.S. Malinova, Influence of inelastic buckling on low-cycle fatigue degradation of reinforcing bars, Constr. Build. Mater. 94 (2015) 644–655, https://doi.org/10.1016/j.conbuildmat.2015.07.102.
[63] L.L. Dodd, J.I. Restrepo-Posada, Model for predicting cyclic behavior of reinforcing steel, J. Struct. Eng. 121 (1995) 433–455.
[64] M.M. Kashani, A.J. Crewe, N.A. Alexander, Nonlinear cyclic response of corrosion-damaged reinforcing bars with the effect of buckling, Constr. Build. Mater. 41 (2013) 388–400, https://doi.org/10.1016/j.conbuildmat.2012.12.011.
[65] S. Caprili, W. Salvatore, Cyclic behaviour of uncorroded and corroded steel reinforcing bars, Constr. Build. Mater. 76 (2015) 168–186, https://doi.org/10.1016/j.conbuildmat.2014.11.025.
[66] W. Zhang, X. Song, X. Gu, S. Li, Tensile and fatigue behavior of corroded rebars, Constr. Build. Mater. 34 (2012) 409–417, https://doi.org/10.1016/j.conbuildmat.2012.02.071.
[67] Toader B., Filippou F.C., Popov E.P. Hysteretic model of ordinary and high-strength reinforcing steel. n.d.
[68] Y.G. Du, L.A. Clark, A.H.C. Chan, Residual capacity of corroded reinforcing bars, Mag. Concr. Res. 57 (2005) 135–147.
[69] a H.C. Chan, L.A. Clark, Y.G. Du, Effect of corrosion on ductility of reinforcing bars, Mag. Concr. Res. 57 (2005) 407–419.
[70] M.M. Kashani, P. Alagheband, R. Khan, S. Davis, Impact of corrosion on low-cycle fatigue degradation of reinforcing bars with the effect of inelastic buckling, Int J. Fatigue 77 (2015) 174–185, https://doi.org/10.1016/j.ijfatigue.2015.03.013.
[71] M.M. Kashani, S. Cai, S.A. Davis, P.J. Vardanega, Influence of bar diameter on low-cycle fatigue degradation of reinforcing bars, J. Mater. Civ. Eng. (2019) 31, https://doi.org/10.1061/(ASCE) MT.1943-5533.0002637.
[72] C.F. Scribner, Reinforcement buckling in reinforced concrete flexural members, ACI J. (1986) 966–973.
[73] Papia M., Russo G., Zingone G. Instability Of Longitudinal Bars In Rc Columns. n.d.
[74] S.J. Pantazopoulou, Detailing for reinforcement stability in RC members, J. Struct. Eng. 124 (1998) 623–632.
[75] F. Vecchi, B. Belletti, Capacity assessment of existing RC columns, Buildings 11 (2021), https://doi.org/10.3390/buildings11040161.
[76] M.M. Kashani, L.N. Lowes, A.J. Crewe, N.A. Alexander, A multi-mechanical nonlinear fibre beam-column model for corroded columns, Int. J. Struct. Integr. 7 (2016), https://doi.org/10.1108/IJSI-09-2014-0044.
[77] M.M. Kashani, L.N. Lowes, A.J. Crewe, N.A. Alexander, Nonlinear fibre element modelling of RC bridge piers considering inelastic buckling of reinforcement, Eng. Struct. 116 (2016), https://doi.org/10.1016/j.engstruct.2016.02.051.
[78] M.M. Kashani, M.R. Salami, K. Goda, N.A. Alexander, Non-linear flexural behaviour of RC columns including bar buckling and fatigue degradation, Mag. Concr. Res. 70 (2018) 231–247, https://doi.org/10.1680/jmacr.16.00495.
[79] M.M. Kashani, C. Málaga-Chuquitaype, S. Yang, N.A. Alexander, Influence of non-stationary content of ground-motions on nonlinear dynamic response of RC bridge piers, Bull. Earthq. Eng. 15 (2017) 3897–3918, https://doi.org/10.1007/s10518-017-0116-8.
[80] R.P. Dhakal, J. Su, Design of transverse reinforcement to avoid premature buckling of main bars, Earthq. Eng. Struct. Dyn. 47 (2018) 147, https://doi.org/10.1002/eqe.2944.
[81] M.M. Kashani, A.J. Crewe, N.A. Alexander, Use of a 3D optical measurement technique for stochastic corrosion pattern analysis of reinforcing bars subjected to accelerated corrosion, Corros. Sci. 73 (2013) 208–221, https://doi.org/10.1016/j.corsci.2013.03.037.
[82] M.J. Moyer, M.J. Kowalsky, Influence of tension strain on buckling of reinforcement in concrete columns, Acids Struct. J. 100 (2003) 75–85.
[83] Y. Feng, M.J. Kowalsky, J.M. Nau, Finite-element method to predict reinforcing bar buckling in RC structures, J. Struct. Eng. 141 (2015), https://doi.org/10.1061/(asce)st.1943-541x.0001048.
[84] X. Ge, M.S. Dietz, N.A. Alexander, M.M. Kashani, Nonlinear dynamic behaviour of severely corroded reinforced concrete columns: shaking table study, Bull. Earthq. Eng. 18 (2020) 1417–1443, https://doi.org/10.1007/s10518-019-00749-3.